

# Breath-by-breath measurement of oxygen using a compact optical sensor

**Conor S. Burke**

**John P. Moore**

**Dorota Wencel**

**Aisling K. McEvoy**

Dublin City University  
National Centre for Sensor Research  
Optical Sensors Laboratory  
Glasnevin, Dublin 9  
Ireland  
E-mail: conor.burke@dcu.ie

**Brian D. MacCraith**

Dublin City University  
Biomedical Diagnostics Institute  
Glasnevin, Dublin 9  
Ireland

**Abstract.** We report on the development of a novel optical oxygen sensor for breath monitoring applications using the technique of phase fluorometry. The principal design criteria are that the system be compact, lightweight, and employ a disposable sensing element (while performing competitively with current commercial analyzers). The oxygen-sensitive, luminescent ruthenium complex  $\text{Ru}[\text{dpp}]_3^{2+}$  is encapsulated in a sol-gel matrix and deposited onto a custom-designed, polymer sensor chip that provides significantly improved luminescence capture efficiency. The performance of the sensor module is characterized using a commercially available lung simulator. A resolution of 0.03%  $\text{O}_2$  is achieved, which compares well with commercial breath monitoring systems and, when combined with its immunity to humidity and ability to respond effectively across a broad range of breathing rates, makes this device an extremely promising candidate for the development of a practical, low-cost budiagnostic tool. © 2008 Society of Photo-Optical Instrumentation Engineers. [DOI: 10.1117/1.2870092]

Keywords: oxygen sensor; breath monitoring; sol-gel; luminescence; phase fluorometry.

Paper 07198R received May 30, 2007; revised manuscript received Sep. 12, 2007; accepted for publication Sep. 13, 2007; published online Feb. 26, 2008.

## 1 Introduction

The ability to measure whole body oxygen consumption has broad clinical applications in occupational health, clinical medicine, and sport. Due to the fact that all processes of metabolism ultimately depend on biological oxidation, the rate of oxygen consumption is a good indicator of overall metabolic rate.

Breath monitoring is an attractive technique for the measurement of  $\text{O}_2$  consumption, as it facilitates real-time monitoring of the inspired and/or expired gas concentration in a noninvasive manner.<sup>1</sup> However, current breath monitoring techniques generally involve the use of large, cumbersome analyzer systems normally located in research or clinical environments. This prevents the use of such systems for routine analysis, such as aiding in the detection and prevention of cardiovascular and metabolic diseases, or the design of effective cardiac rehabilitation and weight loss programs.

The development of a lightweight, portable, low-cost system for the measurement of oxygen in breath would enable the use of this fundamental information in a routine manner by a variety of healthcare professionals including physicians, cardiologists, endocrinologists, dieticians, and exercise specialists. In addition, such a system could facilitate a greater emphasis on preventative healthcare. This would represent a significant innovation in a rapidly growing global market.

We report on the development and preliminary performance of a compact, low-cost optical sensor designed to meet the demands mentioned. The system uses the well-established optical sensing technique of phase fluorometry,<sup>2-5</sup> which facilitates indirect monitoring of changes in the lifetime of an oxygen-sensitive, luminescent complex. The most significant features of this sensor are high sensitivity to oxygen in the required concentration range, a novel optical design for enhanced luminescence capture, and insensitivity to changes in relative humidity (RH). These features combine to deliver an extremely powerful budiagnostic tool for breath gas analyses.

## 2 Background

The sensor developed for this work is based on the oxygen-sensitive, luminescent ruthenium complex, ruthenium-tris(diphenylphenanthroline) [i.e.,  $\text{Ru}[\text{dpp}]_3^{2+}$ ]. We have employed this complex extensively in the past as the basis for a variety of oxygen sensors,<sup>2,5</sup> and among its advantages are long unquenched luminescence lifetime (approximately 5  $\mu\text{s}$ ), high quantum efficiency ( $\sim 0.5$ ), and large Stokes' shift ( $\sim 160$  nm). Furthermore, this complex is compatible with low-cost, blue LED excitation sources and can be encapsulated in a variety of solid porous matrices in a straightforward manner.

The oxygen sensing mechanism is described by the Stern-Volmer equation:

Address all correspondence to Conor Burke, National Centre for Sensor Research, Optical Sensors Laboratory, Dublin City University - Glasnevin, Dublin 9, n/a n/a Ireland; Tel: +353(0)1700 8061; Fax: +353(0)1700 8021; E-mail: conor.burke@dcu.ie

$$I_0/I = \tau_0/\tau = 1 + K_{SV}[O_2], \quad (1)$$

where  $K_{SV}$  is the Stern Volmer constant,  $[O_2]$  is the oxygen concentration, and the term  $I_0/I$  corresponds to the ratio of the maximum fluorescence intensity, i.e., that obtained for 0% oxygen, relative to the fluorescence intensity at each oxygen concentration. Similarly, the term  $\tau_0/\tau$  corresponds to the ratio of the maximum fluorescence lifetime relative to the lifetime at each oxygen concentration. In this work, the technique of phase fluorometry was employed to indirectly monitor the lifetime of the luminescent complex, as opposed to its emission intensity (this technique is described in Sec. 3.2). The sensitivity of such an oxygen sensor is determined by  $K_{SV}$ , which is dependent on the diffusion coefficient (and therefore, the porosity) of the sensor matrix. The use of a sol-gel material as the host matrix offers further advantages in terms of sensor development, as the versatility of the sol-gel process enables tailoring of the physico-chemical properties of the sensing matrix such as porosity, refractive index, and polarity through the correct choice of precursors.<sup>6–8</sup> For example, it is possible to tune the sensitivity of sol-gel-based optical oxygen sensors to the concentration range of interest by selecting a suitable precursor. The choice of precursor also has a significant impact on the humidity sensitivity of the sensor (see Sec. 4.2), which has obvious implications for reliable sensor operation in a humid breath flow. In addition, sol-gel materials are compatible with a wide variety of film deposition techniques such as dip coating, spin coating, knife coating, pin printing, and ink-jet printing. These factors combine to make such materials an attractive choice for the development of a versatile, mass-producible optical sensor platform.

A key feature of the sensor platform is its ability to facilitate the highly efficient detection of luminescence from a thin film. A previous study by us has shown that the emission from luminophores located at or near a dielectric interface is preferentially radiated into the substrate over a range of precisely defined angles, a large fraction of which are greater than the critical angle defined by the refractive indices of the substrate and environment.<sup>9</sup> Consequently, in the case of a conventional, planar substrate, a significant portion of the emitted luminescence is totally internally reflected at the interface between the substrate and the environment, with the result that it is guided away from any photodetector positioned above or below the substrate. The optical chip employed here bears integrated frustrated cones, onto which the luminescent sensor material is deposited. These structures act to *redirect* the emitted luminescence onto a detector positioned beneath the chip, which results in significantly improved collection efficiency, and therefore, improved sensor performance.<sup>10,11</sup> The design is compatible with polymer microfabrication techniques such as injection molding, facilitating the mass production of disposable sensor chips, and making it particularly attractive for this application.

### 3 Experiment

#### 3.1 Sol-Gel-Based Sensor Preparation

Oxygen-sensitive sol-gels were prepared by acid-catalyzed hydrolysis and condensation of the precursor propyltriethoxysilane (PTEOS). In a typical preparation, PTEOS was combined with absolute ethanol, followed by drop-wise addition

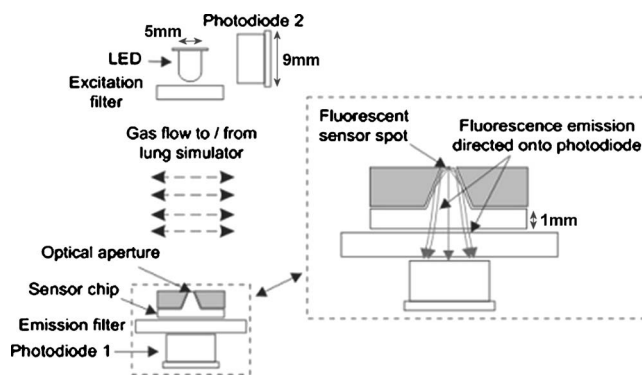


Fig. 1 Optical configuration of the sensor module. Inset shows the principle of operation of the sensor chip.

of aqueous hydrochloric acid at pH 1. The mixture was then stirred for 20 min. An ethanolic solution of  $[Ru(dpp)_3]^{2+}$  was subsequently added to the sol to give a final dye concentration of 2.5 g/l with respect to the total volume of the solution. The final mixture was magnetically stirred under ambient conditions and aged for several weeks before use. All chemicals were purchased from Sigma-Aldrich, Ireland, with the exception of the  $[Ru(dpp)_3]^{2+}$  complex, which was synthesized at the National Centre for Sensor Research, Dublin.

#### 3.2 Optical Sensor Module

A schematic of the optical configuration employed in the breath analyzer is shown in Fig. 1. The central element of the system is an injection-molded, polycarbonate sensor chip that was specifically designed and fabricated in-house for the efficient collection of luminescence from a thin sensor film. The chip consists of a frustrated cone structure that serves to redirect the anisotropic luminescence emission onto a photodetector positioned beneath the chip. Such a design can yield a significant ( $\geq 25$ -fold) increase in the intensity of the collected luminescence compared with a conventional, planar chip.<sup>10</sup> This has considerable implications for the design of low-cost, efficient sensors, and such technology is ideal for this application, combining a high degree of sensitivity with a disposable sensor element.

The portable, low-cost nature of the system is further enhanced through the use of a 5-mm-diam blue LED light source ( $\lambda_{max}=450$  nm, Roithner Lasertechnik, Austria) and a 8-mm Si PIN photodiode detector (S1223-01, Hamamatsu Photonics, United Kingdom). The LED provides direct excitation of a sensor spot that is deposited onto the upper surface of the frustrated cone, which directs the oxygen-sensitive, luminescence emission from the spot onto the active area of the photodiode (photodiode 1). A blue additive dichroic filter (Edmund Optics, United Kingdom) was placed in front of the LED, and a long-pass emission filter with a cut-on wavelength of 550 nm (Thorlabs, Newton, New Jersey) was placed between the sensor chip and photodiode to provide spectral discrimination of the excitation and emission signals. Background light levels at the detector were further reduced through the use of an optical aperture, which ensured that only the coated upper surface of the frustrated cone was exposed to the excitation radiation. The LED output was sinusoidally modulated at a frequency of 20 kHz, and the result-

ant, modulated luminescence emission was detected at the photodiode. Dedicated phase fluorometric detection electronics that were designed in-house were used to detect the phase shift between the excitation and emission signals, which is related to the lifetime of the luminescent complex, as shown in Eq. (2)

$$\tan \phi = 2\pi f\tau. \quad (2)$$

Here,  $\phi$  represents the measured phase angle,  $f$  is the LED modulation frequency, and  $\tau$  is the luminescence lifetime. Changes in the lifetime of the luminescent ruthenium complex due to quenching by oxygen could, therefore, be detected as a change in the output phase angle, this being the principle of phase fluorometry. A second photodiode (photodiode 2) may be positioned adjacent to the LED to provide a reference signal measurement if required.

### 3.3 Deposition of Sensor Spots

The geometry of the substrate necessitates the use of a patterning technology that facilitates the deposition of discrete spots of material. Consequently, printing techniques are an ideal choice for sensor film deposition. Two techniques were investigated poly(dimethylsiloxane) (PDMS) stamp printing and high-precision pin printing, both of which are described in the following sections.

#### 3.3.1 Poly(dimethylsiloxane) stamp printing

This technique involves the use of a poly(dimethylsiloxane) (PDMS) patterning element to transfer the printable material to the substrate. This can be seen as a form of microcontact printing ( $\mu$ CP), which is one of the soft lithographic techniques developed by the Whitesides group at Harvard. The fabrication of such PDMS elements, or stamps, has been described extensively elsewhere, as they play a central role in soft lithographic techniques.<sup>12</sup>

In the work reported here, a circular PDMS stamp with a diameter of 1 mm was used to deposit the liquid sensor sol material onto the upper surface of the frustrated cone. The material was then cured at a temperature of 110°C for 17 h to form a solid sensor film.

#### 3.3.2 Pin printing

Although it is a low-cost, straightforward deposition technique, one significant disadvantage of PDMS stamp printing is a lack of reproducibility in the deposited sensing layers. To improve this aspect of sensor fabrication, the technique of high-precision, automated pin printing was investigated as an alternative.

The apparatus used was a Cartesian Technologies Micro-Sys 5100 MicroArrayer (Genomic Solutions, United Kingdom). The patterning element in this system is a stainless steel pin with a hollow core that acts as a reservoir for the printable material. The pin was immersed in a microwell containing the sensor material, which filled the internal reservoir by capillary action. The pin was then translated from the well to the pre-programmed printing position, where it was then brought into contact with the substrate, and dispensed the volume of sensor material held within the internal reservoir. With this device, it

was possible to deposit uniform sensor spots measuring approximately 100  $\mu$ m in diameter onto the upper surface of the frustrated cone.

### 3.4 Steady-State Characterization Setup

To achieve accurate temperature calibration of the sensors produced for this application, it was necessary to characterize their response over the relevant oxygen concentration range at a series of different gas temperatures. A gas delivery setup comprising mass flow controllers (MFCs, Celerity, Ireland) for oxygen and nitrogen (the carrier gas), and an air process heater (Radionics, Ireland) was employed to this end. The MFCs were controlled using custom-written LabVIEW software (National Instruments, United Kingdom), and the gas temperature was varied by applying a range of different voltages to the air process heater. For the purposes of a typical sensor calibration, the optical module was placed in a custom-made gas cell, which was connected to the gas delivery setup. The temperature within the cell was recorded using a thermistor (BetaTherm, Ireland), the data from which were transmitted along a separate input channel of the detection electronics.

A similar experimental arrangement was employed when characterizing the humidity sensitivity of the sensors, the primary difference being the inclusion of water-filled, gas wash-bottles (AGB Scientific, Ireland) in the gas delivery system. These served to humidify the sample gas flow. All sensor data (including temperature) were recorded using a custom-written LabVIEW program.

### 3.5 Breath Simulation Apparatus

The ability to characterize sensor response across a broad range of breath rates in a reproducible manner was an integral aspect of the work reported here. A commercially available metabolic calibration unit (VacuMed, Ventura, California) was employed to this end. This device is essentially a lung simulator, which mimics oxygen consumption through the dilution of an inspired volume of ambient air with a mixture of carbon dioxide in nitrogen (referred to as the calibration gas). The flow of calibration gas is controlled using a needle valve and monitored using a digital mass flow meter. Breathing is simulated by a motorized piston, which draws ambient air plus the calibration gas into a drum, and then expels the resultant mixture. The breath rate is user adjustable and can be varied from approximately 8 breaths per minute to 60 breaths per minute.

For this work, the sensor module was attached to the outlet of the lung simulator and its response to changes in oxygen concentration was recorded over a range of breath rates using the LabVIEW software mentioned in the previous section.

## 4 Results and Discussion

### 4.1 Steady-State Calibration of Stamp-Printed Sensors

The steady-state responses of stamp-printed sensors were recorded using the experimental setup described in Sec. 3.4. Sensors were exposed to oxygen concentrations ranging from 15 to 23%, which defines the range of interest for this application, and the response of a typical sample for four different gas temperatures is shown in Fig. 2. The performance of the sensor module can be characterized by a large signal-to-noise ratio (SNR > 1100) and a high degree of response stability

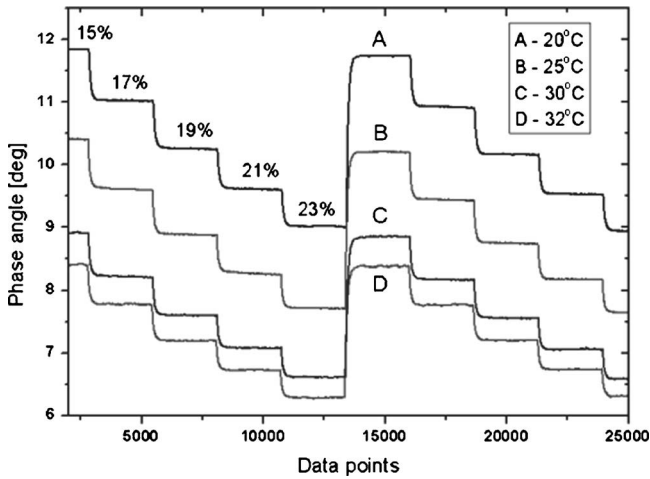


Fig. 2 Steady-state response of stamp-printed oxygen sensor for a range of temperatures.

and repeatability. As the temperature increases, a reduction in sensitivity is apparent, along with a downward shift in the response baseline. These and similar data were subsequently used to yield the 3-D calibration surface shown in Fig. 3 (generated using Table Curve 3D, Systat Software Incorporated, San Jose, California), which is described by the third-order polynomial equation ( $R^2=0.9995$ )

$$O_2[\%] = a + b/\phi + cT + d/\phi^2 + eT^2 + fT/\phi + g/\phi^3 + hT^3 + iT^2/\phi + jT/\phi^2, \quad (3)$$

where  $\phi$  is the recorded phase angle,  $T$  is the temperature, and  $a$  to  $j$  are constants.

#### 4.2 Effect of Humidity on Sensor Performance

Having demonstrated the ability of the sensor to respond effectively over the  $O_2$  concentration range of interest, it was necessary to investigate the degree to which its performance was affected by changes in ambient humidity. The results of these experiments would have a significant influence in determining the suitability of this device for breath monitoring applications.

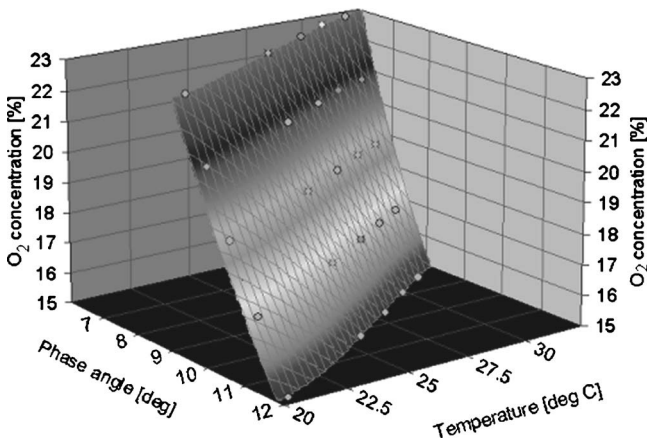


Fig. 3 Calibration surface for a typical stamp-printed sensor.

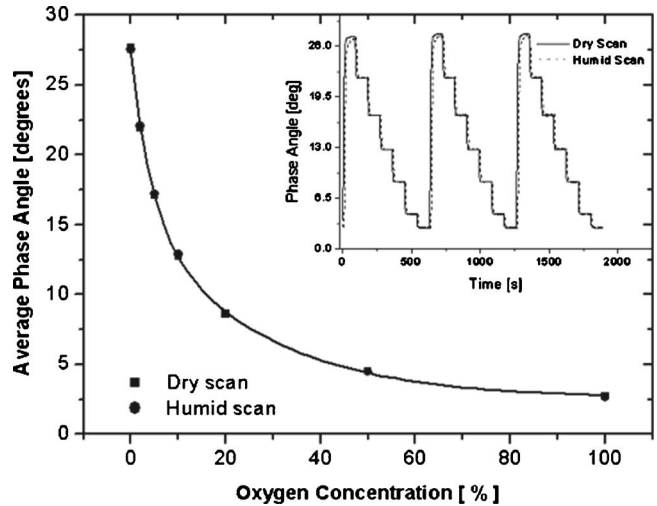


Fig. 4 Calibration curves of a typical PTEOS-derived sensor for both dry (■) and humid (●) gas flows. Inset shows step-by-step response of the sensor to varying  $O_2$  concentrations.

A typical sensor was exposed to both dry and humid mixtures of  $O_2$  in  $N_2$ , as described in Sec. 3.4. Figure 4 illustrates the calibration curves of the sensor when exposed to both dry (■) and humid (●) gas flows. Here, the term “dry” refers to gas having a RH value of less than 5%, while “humid” implies a RH value of greater than 95%. It is clear that, for these two extremes, the sensor calibration curves differ minimally, demonstrating the high degree of RH independence displayed by the doped host matrix for  $O_2$  concentrations ranging from 0 to 100%. This is an extremely significant result in the context of developing a breath gas analyzer, as it facilitates the development of a system that does not require the integration of gas drying or sample heating strategies into its design to eliminate the effects of humid breath.

These preliminary experiments demonstrated the obvious potential of this sol-gel-based sensor for the detection of oxygen in breath. The following stage in this work was the analysis of the sensor performance on a breath-by-breath basis.

#### 4.3 Breath-by-Breath Performance

The sensor module was attached to the output of the lung simulator, and its performance was characterized at a breathing rate of ten breaths per minutes for a 2% change in oxygen concentration. The sensor output was then calibrated using the third-order polynomial described in Sec. 4.1. The resultant, temperature-calibrated response is shown in Fig. 5. Here, the ability of the sensor to respond to changes in  $O_2$  concentrations on a breath-by-breath basis is clearly demonstrated, but the true strength of the device lies in its ability to record the *in-breath*  $O_2$  profile, a characteristic that is lacking in commercial analyzers. The sensor displays a resolution of approximately 0.03%  $O_2$  and clearly detects the expected 2% change in  $O_2$  concentration.

However, closer examination of the data indicates an apparent limitation of the sensor response time, as evidenced by the shape of the response curve for the higher oxygen concentration. This corresponds to the inspiratory cycle of the simulator, where the sensor spot is being exposed to ambient air.

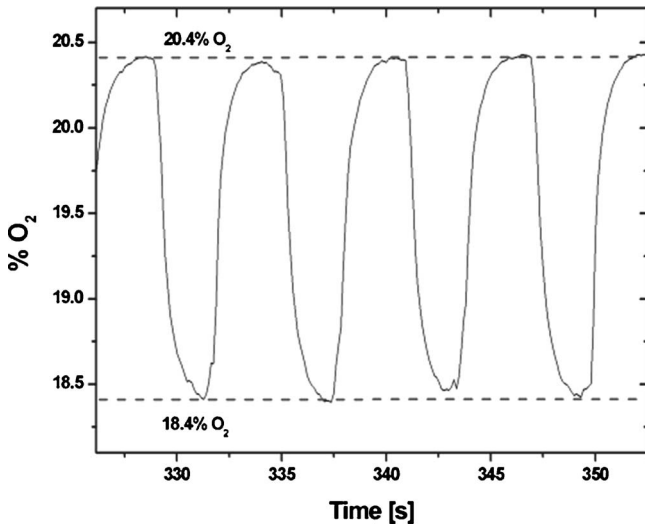


Fig. 5 Temperature-calibrated response of stamp-printed sensor to simulated breath.

The absence of a stable baseline, or plateau in the sensor output, is indicative of incomplete diffusion of oxygen into the sol-gel sensor matrix before the subsequent expiratory cycle of the simulator. This effect is even more apparent for the expiratory cycle of sensor response, i.e., the cycle corresponding to the diffusion of O<sub>2</sub> molecules out of the sensor matrix. This is consistent with the response and recovery characteristics of such sol-gel films, and would appear to suggest that the sensor response time is inadequate at this breathing rate. Given that the response shown was recorded at the relatively low breathing rate of 10 breaths per minute, it was decided to examine the sensor performance in terms of the output signal change at higher breathing rates to more fully understand the extent of this limitation.

#### 4.3.1 Investigation of effective measurement range

*Stamp-printed sensor.* Figures 6(a) and 6(b) display the response of a stamp-printed sensor to a 2% change in oxygen concentration at breathing rates of 10 and 30 breaths per minute, respectively. For the purposes of clarity, it is important to note that the sensors were not temperature calibrated for the purposes of these experiments, as this was not necessary to examine their response range. The data are, therefore, displayed in terms of the phase angle produced by the sensor in response to oxygen. This has the effect of inverting the waveform when compared to that displayed in Fig. 6, with lower phase angles corresponding to the inspiratory phase of the simulator (i.e., the reduced lifetime/higher quenching regime).

There is clearly a significant difference between the data recorded for the two breathing rates, with the sensor registering a reduction in overall signal change of 0.09 deg when exposed to the higher breathing rate. This has obvious implications for effective sensor performance, as such a result demonstrates an apparent loss in sensitivity at higher breathing rates. This limitation was thought to be due to the thickness of the sensor spot, a parameter that is intrinsically linked to its response time. When such stamp-printed spots were examined by optical profilometry (Wyko optical profilometer, Veeco Limited, United Kingdom), they were found to be 35 to 45 μm in thickness, which is a direct result of the PDMS stamp-printing technique and the relatively large volume of material that is deposited. Ideally, sensor spots should be less than 1 μm thick to achieve the subsecond response times that are characteristic of such sol-gel-based, oxygen sensors.<sup>5</sup> Clearly, the technique of PDMS stamp printing was not compatible with this criterion, and high-resolution pin printing was therefore examined as an alternative. It was expected that this technique would not only yield thinner sensor spots due to the reduced volume of deposited material, but that its au-

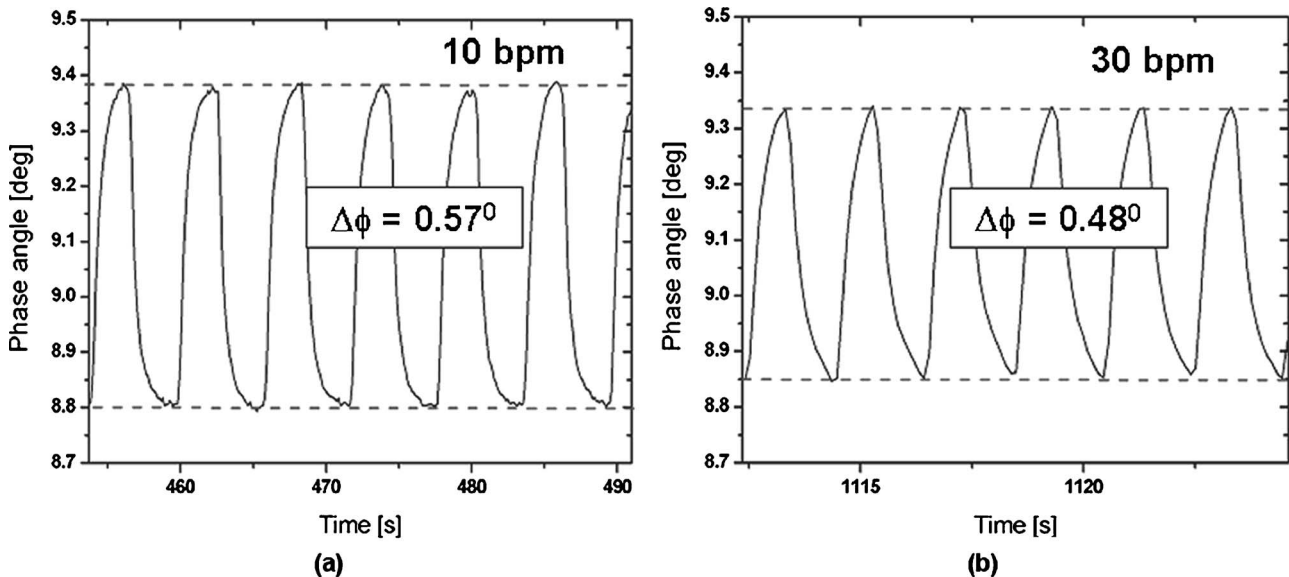


Fig. 6 Response of stamp-printed sensor at breath rates of (a) 10 breaths and (b) 30 breaths per minute.

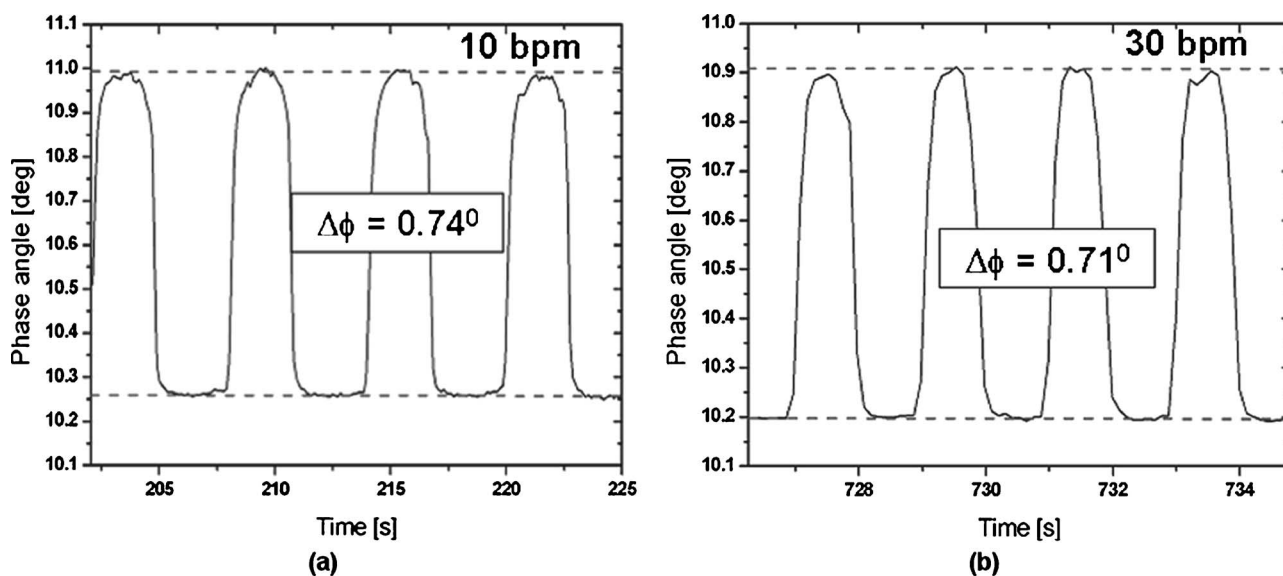


Fig. 7 Response of pin-printed sensor at breath rates of (a) 10 breaths and (b) 30 breaths per minute.

tomated nature would lead to a significant improvement in the reproducibility of sensor spot deposition.

*Pin-printed sensor.* Oxygen-sensitive spots with a diameter of approximately  $100\ \mu\text{m}$  were deposited onto the sensor chips by pin printing, as described in Sec. 3.3.2. Each sample that was investigated consisted of a single sensor spot per frustrated cone. The response of a typical pin-printed chip to a 2% change in  $\text{O}_2$  concentration is shown in Figs. 7(a) and 7(b) for breathing rates of 10 and 30 breaths per minute, respectively. There is a clear improvement in response compared with that of a stamp-printed sample. This is evident in the shape of the waveform, which plateaus during the inspiratory cycle, this being indicative of complete diffusion of oxygen into the sensor film before the expiratory cycle of the simulator. The improvement in response is further reinforced on examination of the apparent sensitivity of the pin-printed sensor at higher breathing rates. The signal change at 30 breaths per minute has reduced by only 0.03 deg, i.e., one third of the reduction recorded for the stamp-printed sensor. On examination by optical profilometry, pin-printed sensor spots were found to be 3 to 4  $\mu\text{m}$  thick, which, as expected, yielded a much improved performance.

Figure 8 illustrates more clearly the relative performances of the stamp- and pin-printed sensors for breathing rates ranging from 10 to 50 breaths per minute. The stamp-printed sensor displays a 40% apparent loss in sensitivity, compared with a loss of just 8% for the pin-printed sensor across the entire range.

In addition, the pin-printed sensor achieves a resolution of 0.03%  $\text{O}_2$  for a 2% change at 10 breaths per minute, demonstrating its ability to not only outperform the stamp-printed sensor in terms of its effective measurement range, but to match its sensitivity at low breathing rates. Such a resolution compares favorably with the 0.05% (vol) quoted for the Oxycon Mobile system supplied by Viasys Healthcare Incorporated (Conshohocken, Pennsylvania), which is the most portable, commercial metabolic gas analyzer that is available at

present.<sup>13</sup> This performance, combined with the additional ability to record the in-breath oxygen profile, emphasizes the potential of the sensor reported here.

## 5 Conclusions

We develop a low-cost, lightweight prototype analyzer for the detection of oxygen in breath on a breath-by-breath basis, and demonstrate its ability to function over a broad range of breathing rates, given a suitable sensor spot deposition technique.

In addition, the humidity-insensitive nature of the sol-gel sensor matrix employed is demonstrated. This characteristic is of vital importance to this application, as it obviates the need for strategies such as breath sample desiccation or heating of the sensor chip in an effort to prevent condensation in the

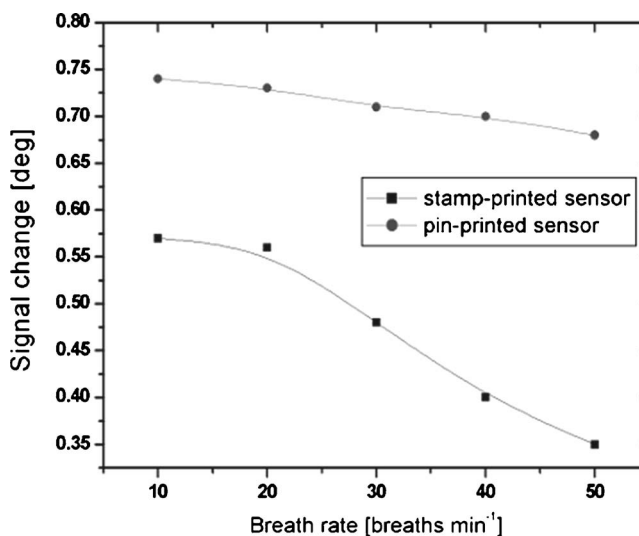


Fig. 8 Comparison of breath rate dependence for stamp-printed (■) and pin-printed (●) sensors.

sensor module. The elimination of such design considerations provides significant scope for the development of a compact, lightweight breath monitoring device. An equally important consequence of their humidity-insensitive nature is that these sensors can be located *directly in the breath flow*, which eliminates complicated sampling strategies and facilitates the measurement of the *in-breath oxygen concentration profile* on a breath-by-breath basis. Such capabilities could afford specialists valuable insights into the processes of oxygen consumption and metabolism in areas such as exercise physiology and preventative healthcare. Its compact, low-cost nature will make it an attractive choice not only for exercise physiology applications (which is envisaged as one of the primary application areas), but also as an additional tool for the clinician in the diagnosis and treatment of conditions such as asthma, diabetes, sleep apnea, and chronic obstructive pulmonary disease (COPD).

An important aspect of the sensor presented here is its generic design, which is compatible with the detection of a wide variety of analytes using fluorescence measurement techniques. In particular, our future work will focus on the ongoing development of a fluorescent carbon dioxide sensor to be integrated into the sensor module along with the current oxygen sensor. This added functionality would facilitate full metabolic analyses of subjects, thereby further increasing the diagnostic power of the system. In addition, it is planned to progress to an optical configuration that is compatible with the deposition of thinner sensor films, while retaining the ability to efficiently capture the anisotropically emitted luminescence. This will facilitate further extension of the device's effective operational range without compromising its efficiency. The sensor performance will then be evaluated in clinical trials.

It is clear, however, that its humidity-insensitive nature and ability to respond across a broad range of breathing rates combine to highlight the potential of this optical sensor for the development of a novel, effective diagnostic platform based on the analysis of oxygen in human breath.

### Acknowledgments

This work was funded by Enterprise Ireland, project code CFTD/03/329.

### References

1. F. Di Francesco, R. Fuoco, M. G. Trivella, and A. Ceccarini, "Breath analysis: trends in techniques and clinical applications," *Microchem. J.* **79**(1-2), 405–410 (2005).
2. C. McDonagh, C. Kolle, A. K. McEvoy, D. L. Dowling, A. A. Cafolla, S. J. Cullen, and B. D. MacCraith, "Phase fluorometric dissolved oxygen sensor," *Sens. Actuators B* **74**(1-3), 124–130 (2001).
3. O. McGaughey, J. V. Ros-Lis, A. Guckian, A. K. McEvoy, C. McDonagh, and B. D. MacCraith, "Development of a fluorescence lifetime-based sol-gel humidity sensor," *Anal. Chim. Acta* **570**(1), 15–20 (2006).
4. M. Valledor, J. Carlos Campo, I. Sanchez-Barragan, J. Carlos Viera, J. M. Costa-Fernandez, and A. Sanz-Medel, "Luminescent ratiometric method in the frequency domain with dual phase-shift measurements: Application to oxygen sensing," *Sens. Actuators B* **117**(1), 266–273 (2006).
5. C. S. Burke, O. McGaughey, J. M. Sabattie, H. Barry, A. K. McEvoy, C. McDonagh, and B. D. MacCraith, "Development of an integrated optic oxygen sensor using a novel, generic platform," *Analyst (Cambridge, U.K.)* **130**(1), 41–45 (2005).
6. C. McDonagh, P. Bowe, K. Mongey, and B. D. MacCraith, "Characterisation of porosity and sensor response times of sol-gel-derived thin films for oxygen sensor applications," *J. Non-Cryst. Solids* **306**(2), 138–148 (2002).
7. C. Malins, T. M. Butler, and B. D. MacCraith, "Influence of the surface polarity of dye-doped sol-gel glass films on optical ammonia sensor response," *Thin Solid Films* **368**(1), 105–110 (2000).
8. R. M. Bukowski, M. D. Davenport, A. H. Titus, and F. V. Bright, "O<sub>2</sub>-responsive chemical sensors based on hybrid xerogels that contain fluorinated precursors," *Appl. Spectrosc.* **60**(9), 951–957 (2006).
9. L. Polerecky, J. Hamrle, and B. D. MacCraith, "Theory of the radiation of dipoles placed within a multilayer system," *Appl. Opt.* **39**(22), 3968–3977 (2000).
10. R. Blue, N. Kent, L. Polerecky, H. McEvoy, D. Gray, and B. D. MacCraith, "Platform for enhanced detection efficiency in luminescence-based sensors," *Electron. Lett.* **41**(12), 682–684 (2005).
11. B. MacCraith and L. Polerecky, "Luminescence-based sensor assembly," U.S. Patent Application No. 2005/0009198 A1 (2005).
12. Y. Xia and G. M. Whitesides, "Soft lithography," *Angew. Chem., Int. Ed.* **37**, 550–575 (1998).
13. See <http://www.viasyshealthcare.com/>.